AIP | Journal of Applied Physics

Graphite fountain: Modeling of growth on transition metals under a thermal gradient

Jongpil Ye and Rodney S. Ruoff

Citation: J. Appl. Phys. **114**, 023516 (2013); doi: 10.1063/1.4812730
View online: http://dx.doi.org/10.1063/1.4812730
View Table of Contents: http://jap.aip.org/resource/1/JAPIAU/v114/i2
Published by the AIP Publishing LLC.

Graphite fountain: Modeling of growth on transition metals under a thermal gradient

Jongpil Ye[1,a)] and Rodney S. Ruoff[2]
[1]*Department of Materials Science and Engineering, Inha University, Incheon 402-751, South Korea*
[2]*Department of Mechanical Engineering and The Texas Materials Institute, 1 University Station C2200, The University of Texas at Austin, Austin, Texas 78712-0292, USA*

(Received 13 February 2013; accepted 17 June 2013; published online 12 July 2013)

We show by modeling that it should be possible to synthesize graphite as a continuous growth in solid metal cylinders under a thermal gradient through the interstitial transport and surface segregation of carbon atoms. Finite-difference-approximation-based calculations show that graphite can continuously grow at the cold end of a 1-cm long cobalt cylinder because of the high interstitial diffusivity and the positive heat of transport of carbon atoms in cobalt. The calculated growth rate can be increased to a few tens of micrometers per minute by varying the carbon concentration and the steady-state temperature profile along the length of the cylinder while maintaining a constant temperature of 1273 K at the hot end of the cylinder. © *2013 AIP Publishing LLC*.
[http://dx.doi.org/10.1063/1.4812730]

I. INTRODUCTION

Graphite has long been in high demand in the steel, automotive, and nuclear industries, among many other applications, and the demand is still growing. Furthermore, in recent years, graphite and its derivatives have attracted much attention as promising materials for various applications, including heat-management components in electronics and electrodes for energy storage devices.[1,2]

Commercial graphite is generally synthesized by mixing and thermally annealing petroleum cokes and coal tar pitch at high temperatures around 3000 K to 3300 K.[3] Uniaxial stress is also applied to pyrolytic carbon sources at such high temperatures in order to synthesize highly ordered pyrolytic graphite (HOPG).[4] Various methods of synthesizing graphite have been discussed in the literature. For example, it has previously been reported that single-crystal graphite can be synthesized by cooling molten metal containing dissolved carbon and precipitating carbon atoms onto the metal surface or by heating single-crystal aluminum carbide and evaporating aluminum atoms.[5,6] These processes also involve heating at high temperatures in the range 2500–3000 °C. However, using chemical vapor deposition (CVD) processes on transition metal substrates could decrease the growth temperature to around 1000 °C.[7,8] During this type of "CVD," graphite actually grows through segregation of supersaturated carbon atoms on the surface of a specimen as it cools. Can the efficiency be significantly enhanced in order to apply this growth mechanism to the mass-production of graphite by generating a "graphite fountain" that grows continuously from one end (or side) of a metal substrate? We address this issue in this paper.

During conventional CVD growth, decomposition of hydrocarbons and segregation of supersaturated carbon atoms occur at the same surface of a metal substrate, leading to a low growth rate. The growth rate might be significantly increased by having hydrocarbon gas decompose at the hot end of a specimen and having supersaturated carbon atoms segregate at the cold end such that a temperature gradient develops. Graphite growth in a thermal gradient has been experimentally demonstrated in carbon/molten metal systems.[9] It was shown that carbon atoms diffuse and precipitate at the interface of the colder end of the molten metal (either on the free surface of the molten metal or on the bottom of a crucible used for the molten metal, depending on the direction of the thermal gradient) to form graphite. Systematic computational studies of the growth kinetics of graphite are needed in order to predict and optimize the growth of graphite in a thermal gradient. In this paper, we present numerical analyses of graphite growth on the colder ends of Ni and Co cylinders subjected to a thermal gradient, and we characterize the effects of material and process parameters on the growth rate.

II. MATHEMATICAL MODEL

The coordinate system for our model is shown in Fig. 1. A temperature gradient can be developed along the length of a metal cylinder by supplying heat to one end and withdrawing heat from the other. The thermal conductivities of Ni and Co are sufficiently high that a steady-state temperature profile $T(x)$ can be assumed to develop in a short time. $T(x)$ is given by

$$T(x) = T_H - \left(\frac{T_H - T_C}{L}\right)x, \tag{1}$$

where T_H is the temperature of the hot end, T_C is the temperature of the cold end, L is the length of the cylinder, and x is the distance from the hot end.

After the temperature profile reaches a steady state, the reactor is pressurized with a hydrocarbon gas that decomposes yielding carbon adatoms on the surface of the hot end

a)Author to whom correspondence should be addressed. Electronic mail: jpye@inha.ac.kr

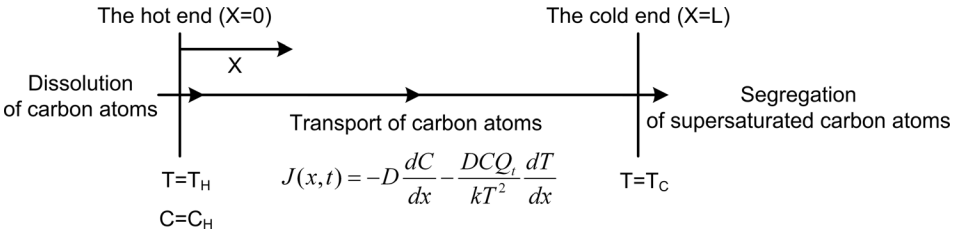

FIG. 1. Coordinate system for model of growth of graphite at the cold end of a solid metal cylinder under a thermal gradient.

of the cylinder. Because of the gradient in concentration and temperature, these carbon adatoms dissolve into the bulk of the cylinder and diffuse by an interstitial mechanism. For such a driving force and mechanism of atomic transport, the atomic flux of carbon atoms is known to be given by

$$J(x,t) = -D\frac{dC}{dx} - \frac{DCQ_t}{kT^2}\frac{dT}{dx}, \tag{2}$$

where k is the Boltzmann constant, and C, D, and Q_t are the concentration, diffusivity, and heat of transport of the carbon atoms, respectively.[10] Equations (1), (2), and the continuity equation give

$$\frac{\partial C}{\partial t} = -\frac{\partial J}{\partial x} = D_0 \exp\left(-\frac{E_d}{kT}\right)\left(\frac{\partial^2 C}{\partial x^2} + \frac{\partial C}{\partial x}\cdot f(x) + C\cdot g(x)\right), \tag{3}$$

where D_0 is the pre-exponential factor, and E_d is the activation barrier for the atomic diffusion. $f(x)$ and $g(x)$ are given as follows:

$$\begin{aligned} f(x) &= -\left(\frac{Q_t + E_d}{kT^2}\right)\left(\frac{T_H - T_C}{L}\right), \\ g(x) &= \frac{Q_t}{k^2T^4}(E_d - 2kT)\left(\frac{T_H - T_C}{L}\right)^2. \end{aligned} \tag{4}$$

Assuming that there is local equilibrium between the gas phase and the surface carbon at the hot end, the boundary conditions for Eq. (3) are set as

$$C(0,t) = C_H, \quad C_H \le C_{sl}(T_H), \tag{5}$$

and

$$J(L,t) = 0, \tag{6}$$

where $C_{sl}(T_H)$ is the solubility limit of carbon at T_H. For these boundary conditions, the concentration of carbon atoms at the hot end of the cylinder is maintained constant and undersaturated. Equation (6) indicates that there is no segregation flux of carbon atoms at the cold end.

The transport of carbon atoms increases the carbon concentration at the cold end. Once the concentration reaches the solubility limit of carbon at the cold end at time t_s, supersaturated carbon atoms begin segregating to the cold surface. The boundary conditions then change as follows:

$$\begin{aligned} &C(0,t) = C_H, \quad C_H \le C_{sl}(T_H), \text{ and} \\ &C(L,t) = C_{sl}(T_C), \end{aligned} \tag{7}$$

where $C_{sl}(T_C)$ is the solubility limit of carbon at T_C.

Thus, the atomic flux at the cold end, $J(L,t)$, becomes nonzero and can be calculated using Eq. (2). The number of segregated carbon atoms per unit surface area is

$$n(t) = \int_{t_s}^{t} J(L,t)dt. \tag{8}$$

If the number of carbon atoms per unit area of graphene is n_g, the number of graphene layers $n_l(t)$ can be expressed as

$$n_l(t) = \frac{n(t)}{n_g}. \tag{9}$$

As the cold end surface is fully covered with monolayer graphene at time t_m, further growth requires the breaking of adhesion between the metal and graphene, leading to a decrease in the segregation flux. If transition state theory is applied to the rate of carbon segregation, the flux of carbon segregation with an energy barrier of E_a is given by

$$J'(L,t) = J(L,t)\exp\left(-\frac{E_a}{kT}\right), \tag{10}$$

where J is the energy-barrier-free segregation flux and E_a is the energy of adhesion between the metal and graphene. Thus, the atomic flux at the cold end after the deposition of a graphene monolayer is as follows:

$$\begin{aligned} J'(L,T) &= J(L,T)\exp\left(-\frac{E_a}{kT}\right) \\ &= \left[-D\left(\frac{dC}{dx}\right) - \frac{DCQ_t}{kT^2}\left(\frac{dT}{dx}\right)\right]_{x=L}. \end{aligned} \tag{11}$$

We presume that the surface of the metal becomes fully covered by a graphene monolayer as the value of the integration reaches the areal atomic density of graphene at time t_m,

$$n(t_m) = \int_{t_s}^{t_m} J(L,t)dt = \frac{4}{3\sqrt{3}a^2}, \tag{12}$$

where a is the atomic spacing in the hexagonal lattice of graphene. After time t_m, the value of $C(L, t)$ can be obtained by solving Eq. (11).

The total number of segregated atoms per unit area at time t can thus be expressed as follows:

$$n(t) = 0 \quad (t \le t_s), \tag{13}$$

$$n(t) = \int_{t_s}^{t} J(L,t)dt \quad (t_s \le t \le t_m), \tag{14}$$

$$n(t) = \int_{t_s}^{t_m} J(L,t)dt + \int_{t_m}^{t} J'(L,t)dt \quad (t \geq t_m). \tag{15}$$

The thickness of the graphite is then given by

$$h(t) = n(t) \cdot \frac{M_g}{\rho_g N_A}, \tag{16}$$

where M_g is the molecular weight of graphite, ρ_g is the density of graphite, and N_A is Avogadro's number.

III. NUMERICAL METHOD

A finite-difference method is used to calculate the time evolution of carbon concentration in the metal cylinder. The first derivative with respect to x in Eq. (3) is approximated using a central difference formula. The second derivative with respect to x and the first derivative with respect to t are approximated using the Dufort-Frankel scheme,

$$\frac{\partial C(x,\,t)}{\partial x} = \frac{C(x+\Delta x,\,t) - C(x-\Delta x,\,t)}{2\Delta x}, \tag{17}$$

$$\frac{\partial C(x,\,t)}{\partial t} = \frac{C(x,\,t+\Delta t) - C(x,\,t-\Delta t)}{2\Delta t}, \tag{18}$$

$$\frac{\partial^2 C(x,t)}{\partial x^2} = \frac{C(x+\Delta x,t) - C(x,t+\Delta t) - C(x,t-\Delta t) + C(x-\Delta x,t)}{(\Delta x)^2}. \tag{19}$$

If these expressions for the partial derivatives are introduced into Eq. (3), the explicit expression for $C(x,\,t+\Delta t)$ is obtained

$$C(x,\,t+\Delta t) = \frac{1}{1+\frac{2D(x)\Delta t}{(\Delta x)^2}} \cdot [C(x,\,t-\Delta t) + 2D(x)\Delta t \cdot (C_{xx}(x,\,t) + C_x(x,\,t) \cdot f(x) + C(x,\,t) \cdot g(x))], \tag{20}$$

where $C_x(x,\,t) = \frac{C(x+\Delta x,t)-C(x-\Delta x,t)}{2\Delta x}$ and $C_{xx}(x,\,t) = \frac{C(x+\Delta x,t)-2C(x,t)+C(x-\Delta x,t)}{(\Delta x)^2}$. By using a backward difference formula for the rightmost first derivative with respect to x, the following expressions are obtained:

$$J(L,t) = -D(L)\left[\frac{C(L,\,t) - C(L-\Delta x,\,t)}{\Delta x} - \frac{C(L,\,t)Q_t}{kT_C^2}\left(\frac{T_H - T_C}{L}\right)\right] = 0, \tag{21}$$

$$C(L,\,t) = \frac{C(L-\Delta x,\,t)}{\left[1 - \frac{Q_t}{kT_C^2}\left(\frac{T_H - T_C}{L}\right)\Delta x\right]}. \tag{22}$$

As the value of $C(L,\,t)$ reaches the solubility limit of carbon, the boundary condition at the cold end changes to

$$C(L,\,t) = C_{sl}(T_C).$$

Thus, the segregation flux is given by

$$J(L,t) = -D(L)\left[\frac{C_{sl}(T_C) - C(L-\Delta x,\,t)}{\Delta x} - \frac{C_{sl}(T_C)Q_t}{kT_C^2}\left(\frac{T_H - T_C}{L}\right)\right]. \tag{23}$$

After Eq. (12) is satisfied, the segregation flux and carbon concentration at the cold end are given by

$$\begin{aligned} J'(L,T) &= -D(L)\exp\left(-\frac{E_a}{kT}\right)\left[\frac{C_{sl}(T_C) - C(L-\Delta x,\,t)}{\Delta x} - \frac{C_{sl}(T_C)Q_t}{kT_C^2}\left(\frac{T_H - T_C}{L}\right)\right] \\ &= -D(L)\left[\frac{C(L,\,t) - C(L-\Delta x,\,t)}{\Delta x} - \frac{C(L,\,t)Q_t}{kT_C^2}\left(\frac{T_H - T_C}{L}\right)\right], \end{aligned} \tag{24}$$

$$C(L,\,t) = \frac{C(L-\Delta x,\,t) - \frac{J'\Delta x}{D(L)}}{\left[1 - \frac{Q_t}{kT_C^2}\left(\frac{T_H - T_C}{L}\right)\Delta x\right]}. \tag{25}$$

The integrations in Eqs. (12), (14), and (15) are performed using the trapezoidal rule.

IV. RESULTS AND DISCUSSION

Numerical simulation was used for calculation of the transport of carbon atoms in Ni and Co, each of which is a representative catalyst for hydrocarbon decomposition. Table I lists the properties of Ni and Co used in the simulation. The solubility limits of carbon in Ni and Co at various temperatures are taken from the FactSage® thermochemical database.[11]

Results of calculations are shown in Figs. 2 and 3. Mean values of heats of transport were used for these calculations. Figs. 2(a) and 2(b) show the changes in carbon concentration in 1-cm long Ni and Co cylinders under a thermal gradient. The changes in carbon concentrations are calculated by solving Eq. (20). For the calculation, T_H and T_C, which denote the temperatures at the hot and cold ends of the cylinders,

TABLE I. List of properties of Ni and Co that are used in simulation.

Property	Ni	Co
Q_t (kJ/mol)[a]	−6.7 ± 5.9 (Ref. 12)	6.3 ± 6.3 (Ref. 12)
E_d (kJ/mol)[b]	167.95 (Ref. 13)	38.5 (Ref. 14)
D_0 (cm^2/s)[c]	2.48 (Ref. 13)	0.53 (Ref. 14)
E_a (eV/atom)[d]	0.10 (Ref. 15)	0.12 (Ref. 15)

[a]Heat of transport of carbon atoms.
[b]Activation energy for interstitial diffusion of carbon atoms.
[c]Pre-exponential factor for interstitial diffusivity of carbon atoms.
[d]Energy of adhesion between fcc(111) surface and graphene.

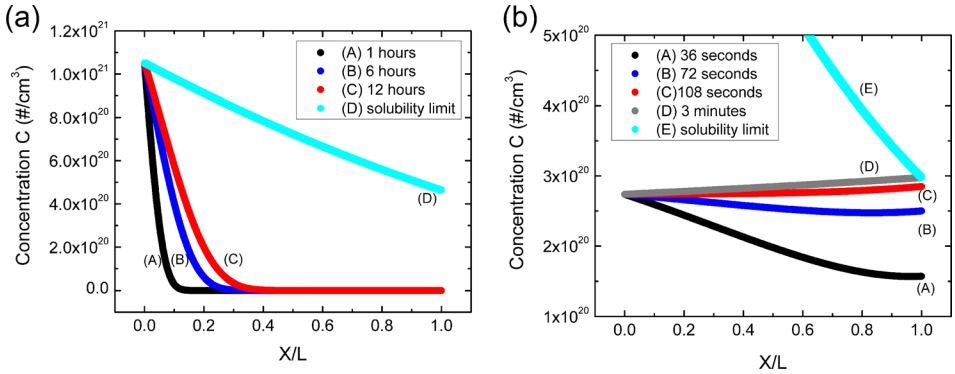

FIG. 2. Change in carbon concentration in (a) Ni and (b) Co. Values of C_H are 1.1372 and 0.3 at. % in (a) and (b), respectively. Solubility limit of carbon in Ni is 1.1372 at. % at 1273 K. This unit is converted to [1/cm^3] by: C_H [1/cm^3] = (C_H [at. %]/100)/{1 − (C_H [at. %]/100)}*($\rho N_A/M$), where ρ is the density of the metal, M is the molecular weight of the metal, and N_A is Avogadro's number.

respectively, are 1273 K and 1073 K. The transport of carbon atoms in the Ni cylinder is so slow that they are still far apart from the cold end of the cylinder after 12 h, even when the carbon concentration at the hot end (C_H) is set equal to the solubility limit, as shown in Fig. 2(a). In contrast, the transport of carbon atoms in the Co cylinder is sufficiently fast that they supersaturate the cold end only in a few minutes, even when the carbon concentration at the hot end (C_H) is set far below the saturation point (i.e., the carbon concentration at the hot end is set equal to 0.3 at. %), as shown in Fig. 2(b). From Eq. (2), an interstitial atom tends to migrate along the direction of a thermal gradient in materials in which the heat of transport of the interstitial atom is positive.[12] Thus, the fast transport of carbon atoms in Co is associated with both the relatively high interstitial diffusivity of carbon atoms in Co and the positive heat of transport of carbon atoms in Co. This result shows that Co may be a more suitable catalyst than Ni for the continuous growth of graphite in a thermal gradient.

Once the cold end of the Co cylinder is supersaturated with carbon atoms, they begin segregating to form graphite on the surface. Fig. 3(a) shows the change in the thickness of the graphite layer over time. The thickness of the graphite layer is calculated using Eqs. (12)–(16). T_H, T_C, and C_H are the same as those used in the analyses whose results are shown in Fig. 2(b). From Fig. 3(a), the thickness of the graphite layer increases linearly with time at a growth rate of about 0.4 μm/min. The growth of the graphite layer is expected to continue uninterrupted as carbon sources could continuously be supplied to the hot end that is undersaturated with carbon atoms.

The growth rate can be controlled by varying either the carbon concentration at the hot end or the steady-state temperature profile along the length of the cylinder. Figure 3(b) shows the effects of these variables on the growth rate of the graphite layer. In these results, the thickness of the graphite layer grown for 30 min is calculated for various values of C_H and T_C. From Fig. 3(b), the growth rate increases with increasing C_H for a given value of T_C, as expected. For each value of C_H, the growth rate exhibits a maximum at a particular value of T_C, each of which is indicated by an empty square in the figure. The maximum rate can be understood in terms of the changes in three parameters including the thermal gradient along the length of the cylinder, the solubility limit of carbon at the cold end of the cylinder, and the diffusivity of carbon atoms. The change in each parameter is due to the change in temperature at the cold end of the cylinder. A decrease in the temperature at the cold end leads to a decrease in the solubility limit of carbon at the cold end and an increase in the thermal gradient along the length of the cylinder. The changes in these parameters increase the segregation flux of carbon atoms at the cold end, as indicated by Eqs. (2) and (11), causing the growth rate to increase. However, as temperature decreases, the diffusivity of carbon atoms also decreases, causing the growth rate to decrease. Because of the contrasting effects of the change in temperature on the growth rate of graphite, the growth rate exhibits a maximum at a particular temperature of the cold end of the cylinder, as shown in Fig. 3(b). It should also be noted that the position of the maximum growth rate shifts toward higher temperatures with increasing carbon concentration at the hot end.

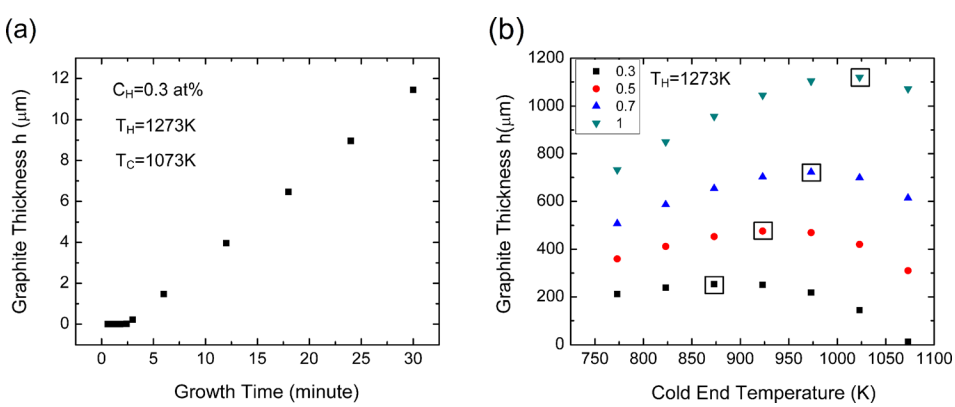

FIG. 3. Graphite thickness plotted as functions of (a) growth time and (b) temperature, at the cold end of the solid cylinder. Legend in inset of (b) indicates carbon concentration at the hot end of the cylinder.

The growth rates vary with the variations in the heats of transport shown in Table I, but their variations are small enough to still confirm that Co can be a catalyst for the continuous growth of graphite in a thermal gradient. For example, the thickness of graphite grown for 30 min is calculated to vary between 997 μm and 1247 μm when C_H and T_C are set to be 1 at. % and 1023 K, respectively. (The thickness is about 1119 μm when the mean value of heat of transport is used as shown in Fig. 3(b). It is indicated by the uppermost empty square.)

These results suggest new process conditions for the continuous and high-throughput growth of graphite on transition metals under a thermal gradient; thus, opening up a new area for future investigation. We expect that extending this model to 3-dimensions will lead to new results on the dependence of graphite growth on, e.g., the shape of the metal piece (solid or hollow cylinder, or other shapes), and other factors.

V. CONCLUSIONS

In summary, we have proposed a model for the growth of graphite on transition metals in a thermal gradient and presented the results of calculations based on finite-difference approximation. The model suggests that growth of graphite could proceed continuously under a thermal gradient through the segregation of carbon atoms at the cold end of a metal cylinder, in particular with cobalt looking more promising than nickel. The continuous growth originates from the high diffusivity and the positive heat of transport of interstitial carbon atoms in Co. The growth rate increases with increasing carbon concentration at the hot end of the cylinder, and there is a particular steady-state temperature profile for which the growth rate is maximized for a given carbon concentration at the hot end. This model should provide a basis for developing a high-throughput method of growing graphite from inexpensive precursors such as methane.

ACKNOWLEDGMENTS

This work was supported by a Keck Foundation Grant (J.Y. and R.S.R.) and an Inha University Research Grant to J.Y. (INHA-44768). We gratefully acknowledge the High Performance Computing Center of the University of Texas at Austin for providing the computing resources used for this work.

[1]S. Ghosh and A. A. Balandin, in *Thermal Properties of Graphene and Carbon Based Materials: Prospects of Thermal Management Applications*, edited by A. A. Baladin, A. Geim, J. Huang, D. Li (Mater. Res. Soc. Symp. Proc., 2011), Vol. 1344, pp. 43–53.
[2]M. Endo, C. Kim, K. Nishimura, T. Fujino, and K. Miyashita, Carbon **38**, 183 (2000).
[3]S. Ragan and H. Marsh, J. Mater. Sci. **18**, 3161–3176 (1983).
[4]A. D. McNaught and A. Wilkinson, *Compendium of Chemical Terminology (The "Gold book")*, 2nd ed. (Blackwell Scientific Publications, Oxford, 1997).
[5]P. C. Li, Nature **192**, 864–865 (1961).
[6]L. M. Foster, G. Long, and H. C. Stumpf, Am. Mineral. **43**, 285–296 (1958).
[7]A. E. B. Presland, Carbon **7**, 1–8 (1969).
[8]S. Robertson, Carbon **10**, 221–222 (1972).
[9]S. B. Austerman, S. M. Myron, and J. W. Wagner, Carbon **5**, 549–557 (1967).
[10]R. W. Balluffi, S. M. Allen, and W. C. Carter, *Kinetics of Materials*, 1st ed. (John Wiley & Sons, New Jersey, 2005).
[11]C. W. Bale, P. Chartrand, S. A. Degterov, G. Eriksson, K. Hack, R. B. Mahfoud, J. Melancon, A. D. Pelton, and S. Peterson, CALPHAD **26**, 189–228 (2002).
[12]J. G. Shaw and W. A. Oates, Metall. Trans. **2**, 2127–2134 (1971).
[13]J. J. Lander, H. E. Kern, and A. L. Beach, J. Appl. Phys. **23**, 1305–1309 (1952).
[14]J. C. Hamilton and J. M. Blakely, Surf. Sci. **91**, 199–217 (1980).
[15]G. Giovannetti, P. A. Khomyakov, G. Brocks, V. M. Karpan, J. van den Brink, and P. J. Kelly, Phys Rev Lett **101**, 026803 (2008).